Rev. Adv. Mater. Sci. 33 (2013) 164-170

FABRICATION AND PHOTOLUMINESCENCE OF THE SnO_2 PLATE-SHAPE NANOSTRUCTURES AND CHRYSANTHEMUM-SHAPE NANOSTRUCTURES

B. Wang[1], I.L. Li[1], P. Xu[1] and L.W. Xing[2]

[1]Shenzhen Key Lab of Mocro-Nano Photonic Information Technology,
College of Electronic Science and Technology, Shenzhen University, Shenzhen 518060, China
[2]CSR Qingdao Sifang CO., LTD, China

Received: October 17, 2011

Abstract. Two new nanostructures, Plate-shape Nanostructures and Chrysanthemum-shape Nanostructures of SnO_2, have been grown on single silicon substrates by Au-Ag alloying catalyst assisted carbothermal evaporation of SnO_2 and active carbon powders (thermal CVD). The morphology and structure of the prepared nanostructures are determined on the basis of scanning electron microscopy (SEM), field-emission scanning electron microscopy (FESEM), energy dispersive spectrum (EDS), X-ray diffraction (XRD) and photoluminescence spectra (PL) analysis. The peak at 343 nm is the band-to-band emission peak and the corresponding band gap of SnO_2 is calculated by using an accurate full-potential linearized augmented planewave method. The new peak at 416 nm in the measured photoluminescence spectra of SnO_2 Plate-shape nanostructures is observed, implying that more luminescence centers exist in SnO_2 Plate-shape nanostructures due to nanocrystals and defects. The growth mechanism of SnO_2 Plate-shape nanostructures and SnO_2 Chrysanthemum-shape nanostructures can be explained on the basis of the vapor–liquid–solid (VLS) processes.

1. INTRODUCTION

It is well known that SnO_2 is an important n-type semiconductor functional material with wide band gap energy, high donor concentration and large mobility [1], which has been widely applied in the field of opto- and microelectronics. For instance, SnO_2 can be utilized in solar cell [2], transparent conducting electrodes [3], gas sensors [4,5], and transistors [6]. Thus, the SnO_2 nanostructures have been utilized as transparent electrodes in sophisticated electronic devices [7–9]. The material also has an advantage in availability of constituent atoms different from ITO (indium tin oxide). Nanostructures of SnO_2 have been prepared by variety of techniques such as reactive sputtering, spray pyrolysis, evaporation, sol-gel, pulsed laser deposition, plasma assisted/enhanced chemical vapor deposition, and thermal chemical vapor deposition (CVD) [10–19]. Among all these, CVD has meaningful advantages such as large area growth, precise control over thickness, and superior conformal coverage [20].

In this paper, we have reported two new kinds of SnO_2 nanostructures, Plate-shape nanostructures and Chrysanthemum-shape nanostructures, which have been grown on single silicon substrates by Au-Ag alloying catalyst assisted carbothermal evaporation of SnO_2 powders (thermal CVD) [21,22]. Additionally, the peak at 343 nm is the band-to-band emission peak and the corresponding band gap of SnO_2 is calculated by using an accurate full-potential linearized augmented planewave method. The new

Corresponding author: B. Wang, e-mail address: wangbing@szu.edu.cn

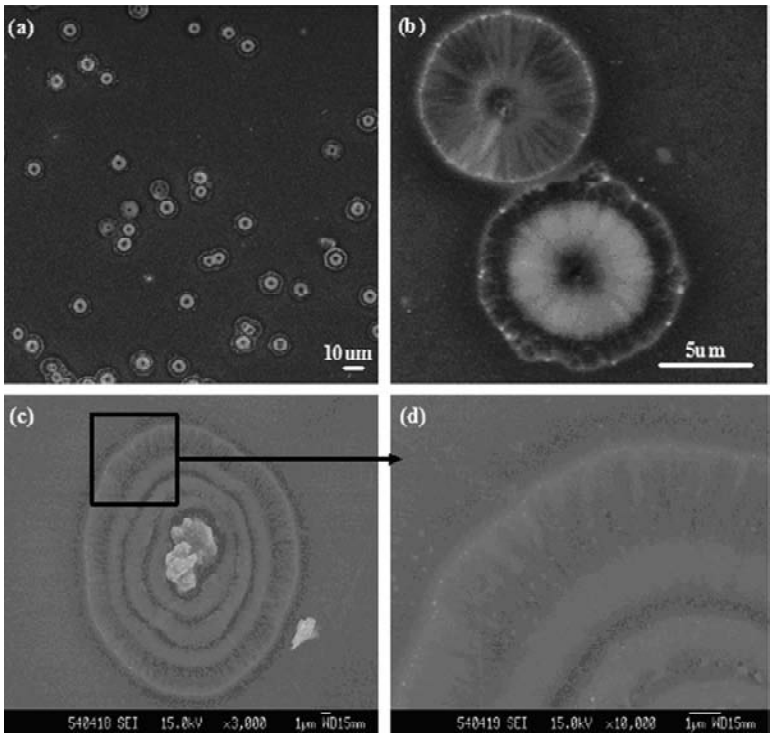

Fig. 1. SEM image (a), (b), and FESEM image (c), (d) of the synthesized SnO_2 Plate-shape nanostructures.

peak at 416 nm in the measured photoluminescence spectra of SnO_2 Plate-shape nanostructures is observed, implying that more luminescence centers exist in SnO_2 Plate-shape nanostructures due to nanocrystals and defects.

2. EXPERIMENTAL

The SnO_2 nanostructures synthesis is minutely depicted as follows. The Au-Ag (atom ratio 1:1) layer (about 10 nm in thickness) is deposited on single silicon (001) substrates with area of 5 mm^2 by sputtering. The active carbon and SnO_2 powders (both 99.99%) are mixed in a 1:4 weight ratio and placed into a small quartz tube. The two Si substrates covered by Au-Ag alloy are put on a ceramic plate near the mixture of carbon and SnO_2 inside the small quartz tube. The distance between two substrates is about 2 cm and substrate 1 is 2 cm away from the mixture of carbon and SnO_2. Then the small quartz tube, with an inner diameter of 2.5 cm, is pulled into the center of a large quartz tube, with an inner diameter of 6 cm, and together they are inserted in a horizontal tube electric furnace. The whole system is evacuated by a vacuum pump for a couple of hours, then, the nitrogen gas is guided into the system at 200 sccm, and the pressure is kept at 800 Torr. Afterwards, the system is rapidly heated up to 750 °C from the room temperature and kept at the temperature for 15 min. Finally, the system is cooled down to the room temperature in several hours. When two substrates are taken from the small quartz, we can see gray production on substrates. Scanning electron microscopy (SEM), field emission scanning electron microscopy (FESEM), energy dispersive spectrum (EDS), X-ray diffraction (XRD) are employed to identify the morphology and structure of the synthesized productions. Room-temperature photoluminescence (PL) is used to characterize the luminescence of SnO_2 nanostructures. Note that we can easily repeat the experimental results, suggesting that our method is flexible and reproducible.

3. RESULTS AND DISCUSSION

Morphologies of the synthesized SnO_2 nanostructures in two substrates are shown as Figs. 1 and 2. From Fig. 1a, many SnO_2 plate-shape nanostructures grown in Substrate 1 in Fig. 1 are clearly seen and the white cirque-shape part exists in most of them. In detailed, the highly-magnified SEM image is displayed in Fig. 1b. Two SnO_2 Plate-shape nanostructures are shown clearly. Both of them present radiate-shape from inside to outside. The edge of the two Plate-shape nanostructures is the white and bright pearl-chain-like structure. The FESEM image of a Plate-shape nanostructure is shown in Fig. 1c. The cirque-shape part in this Plate-shape nanostructure divides into three layer cirques

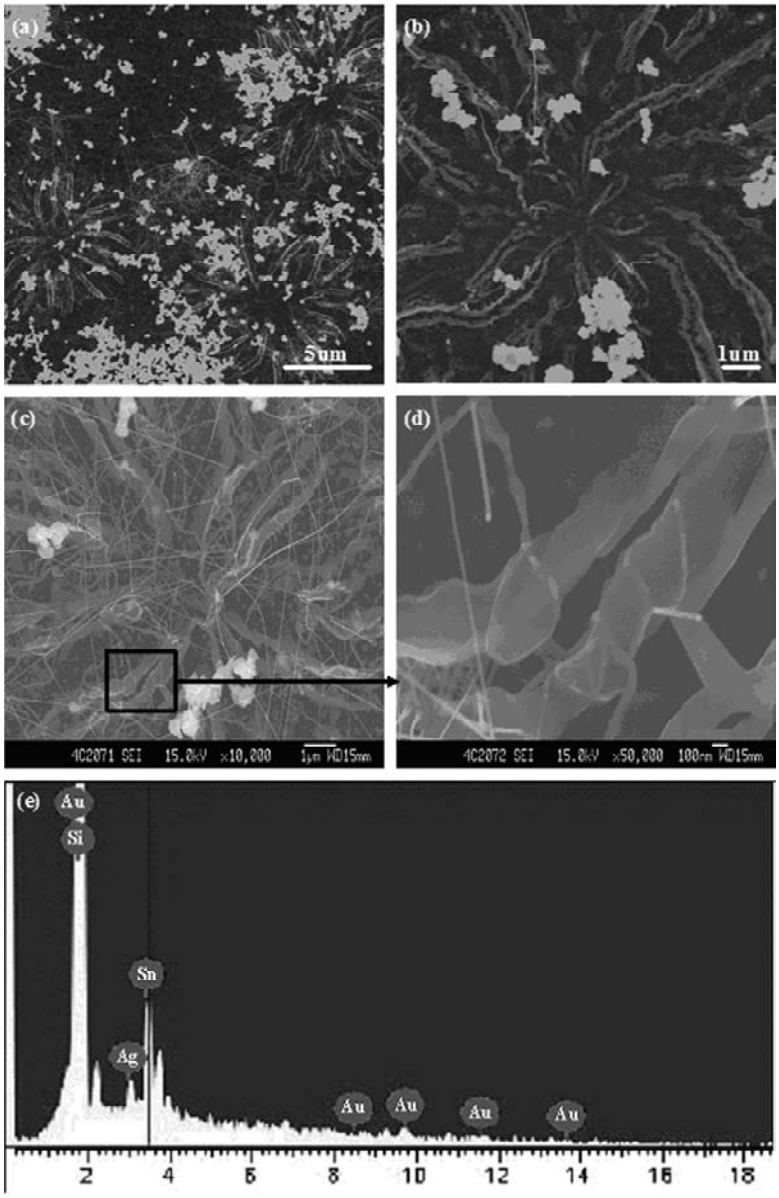

Fig. 2. SEM image (a), (b), and FESEM image (c), (d) of the synthesized SnO_2 Chrysanthemum-shape nanostructures, the EDS of the white powders (e).

radiating from inside to outside. The higher-magnified FESEM image of one section in Fig. 1c is shown in Fig. 1d, from which the three layer cirques radiating from inside to outside are more clearly displayed and some pearl-like dots distribute outside and inside of the edge of the Plate-shape nanostructure.

The SnO_2 Chrysanthemum-shape nanostructures in Fig. 2 are found in the substrate 2. Three Chrysanthemum-shape nanostructures are displayed in Fig. 2a. The EDS pattern (Fig. 2e) recorded at the white powders in Fig. 2a indicates that white powders are Sn (Au, Ag, and Si come from the substrate). The higher-magnified image of one Chrysanthemum-shape nanostructure shown in Fig. 2b indicates that each petal of the Chrysanthemum-shape nanostructure is made up of two pieces of embranchment extending to same direction. The FESEM image of one Chrysanthemum-shape nanostructure in Fig. 2c shows that some nanowires with the diameter of 10-30 nm distribute on the Chrysanthemum-shape nanostructure. The higher-magnified FESEM image of one section in Fig. 2c is shown in Fig. 2d. One petal of the Chrysanthemum-shape nanostructure is made up of two embranchments. In addition, one nanowire with the diameter of 30 nm grows from one embranchment and enwind the embranchment, the other nanowire with the diameter of 30 nm grows from the other embranchment and connects the embranchment, and then both nanowires extend

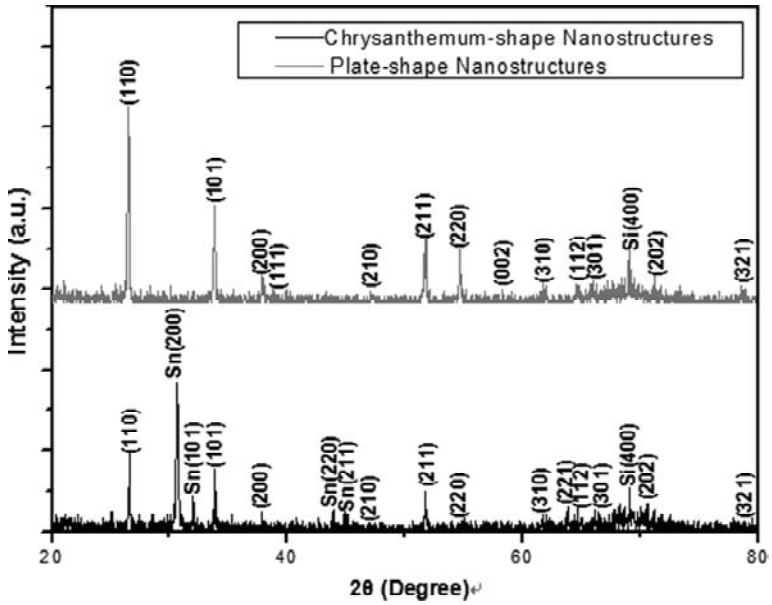

Fig. 3. The XRD pattern of the synthesized two kinds of SnO_2 nanostructures.

outside of the embranchment so that some of these nanowires form net-shape structure and cover the whole Chrysanthemum-shape nanostructure as shown in Fig. 2c.

The X-ray diffraction (XRD) measurement is carried out to identify the crystalline structure of the two kinds of SnO_2 nanostructures and Fig. 3 shows the XRD patterns. Both samples show tetragonal rutile SnO_2 phase with (110), (101), (200), (210), (211), (220), (310), (112), (301), (202), and (321) diffraction peaks, and a highly preferred direction along with (110) direction. The XRD patterns of the samples indicate the crystalline structural parameters can be indexed to the tetragonal rutile structure of SnO_2 with lattice constants of a = 4.738 Å and c = 3.188 Å (JCPDS 21-1250). The Intensity of the peak in the XRD pattern of SnO_2. Plate-shape nanostructures higher than that of SnO_2. Chrysanthemum-shape nanostructures attributes to the thickness of the density of the SnO_2. Plate-shape nanostructures higher than those of the SnO_2 Chrysanthemum-shape nanostructures. In addition, the peak (111) and (002) do not appear in the XRD pattern of the SnO_2 Chrysanthemum-shape nanostructures. The diffraction peak at $2\theta = 69.02°$ is quite broad due to the overlapping with that of Si (400) in both of XRD pattern. In the XRD pattern of the SnO_2 Chrysanthemum-shape nanostructures, body-centered tetragonal β-Sn phase with (200), (101), (220), and (211) diffraction peaks appear too besides the diffraction peaks of SnO_2. The appearance of four diffraction peaks of Sn indicates that the crystalline structural parameters can be indexed to the body-centered tetragonal structure of Sn with lattice constants of a = 5.83 Å, b = 3.18 Å (JCPDS 04-0673). This conclusion means that both SnO_2 and Sn exist in the second sample. According to the EDS result in Fig. 2e, the white powders in Fig. 2a are Sn, so the SnO_2 Chrysanthemum-shape nanostructures is SnO_2.

Photoluminescence of the obtained SnO_2 nanostructures in two samples is investigated at room temperature and the result is shown in Fig. 4. Both of the PL spectra of the SnO_2 Plate-shape nanostructures and that of the SnO_2 Chrysanthemum-shape nanostructures consist of the emission band located at 343, 399, 470, 549, and 575 nm. Firstly, the peak at 343 nm is the band-to-band emission peak of the two kinds of SnO_2 nanostructures, which is originated from the recombination of free exciton electronhole [23]. We also calculated and investigated the band gap of SnO_2 by using an accurate full-potential linearized augmented planewave method in Fig. 5. The calculations were implemented in the latest WIEN2K code [24,25]. From Fig. 5 we can see that SnO_2 have a direct band gap. The band gap is about 3.615 eV which has revised from the experimentation. The reason that the peak is weaker than other peaks is that the peaks caused by defect levels associated with oxygen vacancies or tin interstitials resulting from the size effect of the SnO_2 nanostructures is strong so as to cripple the band-to-band emission peak [26]. Secondly, the appearance of the 399 nm peak is independent of the concentration of oxygen vacancies, while due

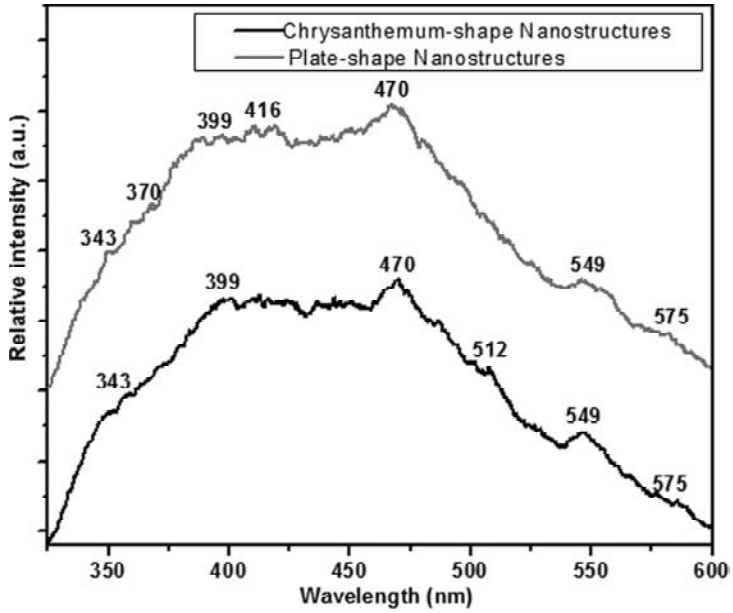

Fig. 4. The room temperature PL spectrum of the synthesized two kinds of SnO_2 nanostructures.

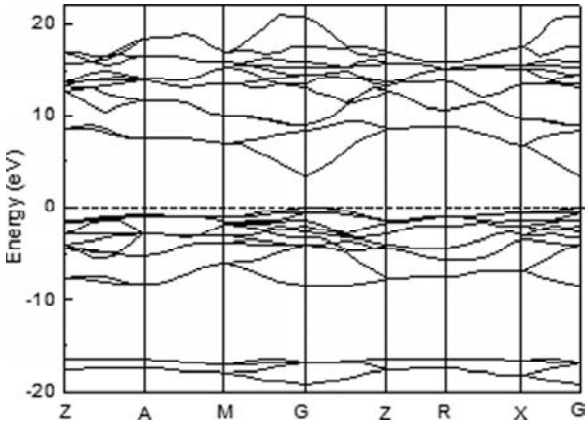

Fig. 5. The band gap of SnO_2 by using an accurate full-potential linearized augmented planewave method.

to structural defects or luminescent centers, such as nanocrystals or defects in the SnO_2 nanostructures [26,27]. Thirdly, the peak at 470 nm is possibly attributed to the electron transition mediated by defect levels such as oxygen vacancies in the band gap [28]. Fourth, the 549, 575 nm peak has been observed in previous report [21,29]. In addition, the PL spectra of the SnO_2 Plate-shape nanostructures consist of the emission band located at 370 and 416 nm. The 370 nm peak is attributed to the band-to-acceptor peak and related to the impurity or defect concentration and not to the structural properties [27]. The 416 nm peak is newly found in our case, should be from new luminescence centers existing in SnO_2 Plate-shape nanostructures, such as nanometer sized crystals and defects [30]. While the PL spectra of the SnO_2 Chrysanthemum-shape nanostructures consist of the emission band located at 512 nm, which is attributed to the concentration of oxygen vacancies [25]. It has been reported that the concentration of oxygen vacancies increases with increasing substrate temperature [31]. These oxygen vacancies are created as the donor level below the conduction band and are the origin of the n-type SnO_2 nanostructures. The intensity of this peak increases with the increasing concentration of oxygen vacancies [27].

The growth mechanism of SnO_2 Plate-shape nanostructures can be explained on the basis of the vapor–liquid–solid (VLS) processes. In experimental, Au in Au-Ag alloy as catalysts is usually used to assist the SnO_2 Plate-shape nanostructures synthesis. The reason that the application of the Au-Ag alloy is that the cost of the Au-Ag alloy is lower than that of the pure Au. SnO_2 powders first react with the active carbon, and then SnO can be produced. Subsequently, the produced SnO decomposes into Sn and SnO_2. Sn droplets are still liquid at the reaction temperature due to the low melting point (231.9 C) and fall on the substrate and form Sn-Au alloyed droplets by reacting with the Au particles [26]. Simultaneously, these Sn-Au alloying droplets can provide the energetically favored sites for the adsorption of SnO_2 vapor, so the SnO_2 dissolves in the Sn-Au alloying droplets, forms state of solid-dissolution and grows bigger and bigger so as to form some island-shape structures along different directions [32]. When neighboring two

islands butting and combining, the bridge forms between two islands and this formation process shows liquid behavior so as to decrease the surface energy. If the surface energy is not relative with the growth direction of the crystal, it will decrease the surface area to the least degree so that the circle-shape crystal structures form with continuous combination of the islands. The concentration of the SnO_2 produced by decomposition of SnO in the centre of the circle-shape crystal structures is relatively high so that SnO_2 begins to nucleate and continuous dissolution of SnO_2 in the Sn-Au alloy results in a supersaturated solution. Ultimately, the SnO_2 nanostructure grows out by precipitation of SnO_2 from the supersaturated droplets. So the SnO_2 Plate-shape nanostructures in Fig. 1 can form.

The growth mechanism of SnO_2 Chrysanthemum-shape nanostructures is similar with that of SnO_2 Plate-shape nanostructures. The different distance of the sample away from the source could lead to the different temperature of substrates, which is one of the main reason causing different synthesized morphologies of SnO_2 nanostructures. Naturally, the different supersaturating degree of alloying droplets plays an important role in the formation of different nanostructures due to different substrate's temperatures [33]. At the Substrate 2, the temperature is relatively low comparing with that of Substrate 1, so the supersaturating degree is relatively high. More and more atomics connect with each other so that big multi-crystal nuclear form. After that, atomics evaporated grow selectively along optimized growth directions so that the SnO_2 Chrysanthemum-shape nanostructures shown in Fig. 2 can be formed.

4. CONCLUSION

Two new SnO_2 nanostructures, Plate-shape nanostructure and Chrysanthemum-shape nanostructure, have been synthesized on single silicon substrates by Au-Ag alloy assisted carbothermal evaporation of SnO_2 and active carbon powders (thermal CVD). The peak at 343 nm is the band-to-band emission peak and the corresponding band gap of SnO_2 is calculated by using an accurate full-potential linearized augmented planewave method. The new peak at 416 nm in the measured photoluminescence spectra of SnO_2 Plate-shape nanostructures is observed, implying that more luminescence centers exist in SnO_2 Plate-shape nanostructures due to nanocrystals and defects.

ACKNOWLEDGEMENTS

This work was supported by National Natural Science Foundation of China (50902097), Three Industry Basic Research Emphasis Project of Shenzhen (JC201104210013A), None Three Industry Basic Research Common Project of Shenzhen (JC201105170694A), Open Project of Shenzhen Key Laboratory of Micro-nano Photonic Information Technology (MN201107), Guangdong Natural Science Foundation of China (9451806001002303), and Foundation for Distinguished Young Talents in Higher Education of Guang dong China (LYM08088). In addition, Dr. I. L. Li is grateful for the financial support from NSFC(10704050) and Fok Ying Tung Educational Foundation (114009). State key laboratory of optoelectronic materials and technologies, School of Physics Science & Engineering, Zhongshan University, Guangzhou 510275, China.

REFERENCES

[1] Z.M. Jarzebski and J.P. Marton // *J. Electrochem. Soc.* **123** (1976) 199C.
[2] S. Ferrere, A. Zaban and B.A. Gsegg // *J. Phys. Chem. B.* **101** (1997) 4490.
[3] Y.S. He, J.C. Cambell, R.C. Murphy, M.F.Arendt and J.S. Swinnea // *J. Mater. Res*. **8** (1993) 3131.
[4] G. Ansari, P. Boroojerdian, S.R. Sainkar, R.N. Karekar, R.C. Alyer and S.K. Kulkarni // *Thin. Solid. Films* **295** (1997) 271.
[5] O.K. Varghese and L.K. Malhotra // *Sens. Actuat. B*. **53** (1998) 19.
[6] X.F. Duan, Y. Huang, Y. Cui, J. Wang and C.M. Leiber // *Nature* **409** (2001) 66.
[7] J. Tamaki, M. Nagaishi, Y. Teraoka, N. Mimura and N. Yamazoe // *Surf. Sci.* **221** (1989) 183.
[8] U. Weimar, K.D. Schierbaum and W. Gopel // *Sens. Actuators. B.* **1** (1990) 93.
[9] S.R. Vishwakarma, Rahmatullar and H.C. Prasad // *Solid. State. Electron.* **36** (1993) 1345.
[10] M. Batzill and U. Diebold // *Prog. Surf. Sci.* **79** (2005) 47.
[11] S.G. Ansari, S.W. Gosavi, S.A. Gangal, R.N. Karekar and R.C. Aiyer // *J. Mater. Sci.: Mater. Electron*. **8** (1997) 23.
[12] N.S. Ramgir, I.S. Mulla and K.P. Vijaymohanan // *J. Phys. Chem. B.* **109** (2005) 12297.

[13] S.G. Ansari, P.Boroojerdian, S.R. Sainkar, R.N. Karekar, R.C. Aiyer and S.K. Kulkarni // *Thin. Solid. Films.* **295** (1997) 271.
[14] M.A. Maki-Jaskari and T.T. Rantala // *Phys. Rev. B.* **65** (2002) 245428.
[15] M. Batzill, K. Katsiev, J.M. Burst and U. Diebold // *Phys. Rev. B.* **72** (2005) 165414.
[16] N. Bertrand, F. Maury and P. Duverneuil // *Surf. Coat. Technol*. **200** (2006) 6733.
[17] S.G. Ansari, M.A. Dar, Y.S. Kim, G.S. Kim, H.K. Seo, G. Khang and H.S. Shin // *Appl. Surf. Sci.* **253** (2007) 4668.
[18] Y.C. Her, J.Y. Wu, Y.R. Lin and S.Y. Tsai // *Appl. Phys. Lett.* **89** (2006) 043115.
[19] P.Y. Liu, J.F. Chen and W.D. Sun // *Vacuum* **76** (2004) 7.
[20] S.G. Ansari, M.A. Dar, M.S. Dhage, Y.S. Kim and H.S. Shin // *J. Appl. Phys*. **102** (2007) 073537.
[21] B. Wang, Y.H. Yang, C.X. Wang and G.W. Yang // *Chem. Phys. Lett.* **407** (2005) 347.
[22] B. Wang, Y.H. Yang, C.X. Wang and G.W. Yang // *J. Appl. Phys*. **98** (2005) 073520.
[23] E.J.H. Lee, C. Ribeiro, T.R. Giraldi, E. Longo and E.R. Leite // *Appl. Phys. Lett*. **84** (2004) 1745.
[24] D. J. Singh // *Phys. Rev. B.* **43** (1991) 6388.
[25] P. Blaha, K. Schwarz, G. K. H. Madsen, D. Kvasnicka and J. Luitz, *WIEN2K* (Technical University of Vienna, Austria, 2001).
[26] T.W. Kimand and D.U. Lee // *J. Appl. Phys*. **88** (2000) 3759.
[27] J. Jeong, S.P. Choi, C. Chang, D.C. Shin, J.S. Park, B.T. Lee, Y.J. Park and H.J. Song // *Solid. State. Commun.* **127** (2003) 595.
[28] F. Gu, S.F. Wang, M.K. Lu, G..J. Zhou, D. Xu and D.R. Yuan // *J. Phys. Chem. B.* **108** (2004) 8119.
[29] B. Wang, Y.H. Yang, C.X. Wang, N.S. Xu and G.W. Yang // *J. Appl. Phys*. **98** (2005) 124303.
[30] S.H. Sun, G.W. Meng, G.X. Zhang, T. Gao, BY. Geng, L.D. Zhang and J. Zuo // *Chem. Phys. Lett.* **376** (2003) 103.
[31] D. Davazoglou // *Thin. Solid. Films*. **302** (1997) 204.
[32] X. H. Liu, D. S. Tang and C. L. Zeng // *Acta Phys. Chim. Sin*. **23** (2007) 361.
[33] A.P. Levitt, *Whisker Technology* (Wiley, New York, 1970).